Available online at www.sciencedirect.com
SCIENCE DIRECT®
Physica D 211 (2005) 193–220
PHYSICA D
www.elsevier.com/locate/physd

New singular solutions of the nonlinear Schrödinger equation

Gadi Fibich[a,*], Nir Gavish[a], Xiao-Ping Wang[b]

[a] *Department of Applied Mathematics, School of Mathematical Sciences, Tel Aviv University, Tel Aviv 69978, Israel*
[b] *Department of Mathematics, The Hong Kong University of Science and Technology, Clear Water Bay, Kowloon, Hong Kong*

Received 3 May 2005; received in revised form 14 August 2005; accepted 15 August 2005
Communicated by J. Lega
Available online 6 September 2005

Abstract

We present numerical simulations of a new type of singular solutions of the critical nonlinear Schrödinger equation (NLS), that collapse with a quasi self-similar ring profile at a square root blowup rate. We find and analyze the equation of the ring profile. We observe that the self-similar ring profile is an attractor for a large class of radially-symmetric initial conditions, but is unstable under symmetry-breaking perturbations. The equation for the ring profile admits also multi-ring solutions that give rise to collapsing self-similar multi-ring solutions, but these solutions are unstable even in the radially-symmetric case, and eventually collapse with a single ring profile. Collapsing ring solutions are also observed in the supercritical NLS.

PACS: 42.65.Jx; 42.65.−k

Keywords: Nonlinear Schrödinger equation; Self-similar solution; Singularity; Collapse; Ring profile; Blowup rate

1. Introduction

The focusing critical nonlinear Schrödinger equation (NLS)

$$i\psi_t(t,x,y) + \Delta\psi + |\psi|^2\psi = 0, \qquad \psi(0,x,y) = \psi_0(x,y), \tag{1}$$

is one of the canonical nonlinear equations in physics, arising in various fields such as nonlinear optics, plasma physics, Bose–Einstein condensates (BEC), and surface waves. In nonlinear optics it models the propagation of intense laser beams in a Kerr medium. In this case, t is the axial coordinate in the direction of propagation, x and

* Corresponding author.
E-mail addresses: fibich@tau.ac.il (G. Fibich), nirgvsh@tau.ac.il (N. Gavish), mawang@ust.hk (X.-P. Wang).
URL: www.math.tau.ac.il/∼fibich (G. Fibich).

0167-2789/$ – see front matter © 2005 Elsevier B.V. All rights reserved.
doi:10.1016/j.physd.2005.08.007

y are the spatial coordinates in the transverse plane, $\Delta = \partial_{xx} + \partial_{yy}$ is the diffraction term and $|\psi|^2\psi$ describes the nonlinear Kerr response of the medium.

We now briefly review NLS theory, for more information, see [1–3]. The NLS (1) has two important conservation laws: *power* (L^2 norm) conservation,

$$N(t) = \int |\psi|^2 \,\mathrm{d}x\,\mathrm{d}y \equiv N(0), \tag{2}$$

and Hamiltonian conservation,

$$H(t) = \int |\nabla\psi|^2 \,\mathrm{d}x\,\mathrm{d}y - \frac{1}{2}\int |\psi|^4 \,\mathrm{d}x\,\mathrm{d}y \equiv H(0). \tag{3}$$

It is well known that solutions of the two-dimensional critical NLS (1) can self-focus and become singular at a finite time T_c. A necessary condition for blowup is that the *initial power* $N(0)$ exceeds a threshold power N_c, i.e., $N(0) \geq N_c$. A sufficient condition for collapse is that the initial Hamiltonian is negative, i.e., $H(0) < 0$.

The two-dimensional NLS (1) has waveguide solutions of the form $\psi = \mathrm{e}^{\mathrm{i}t} R(r)$, where R is the solution of

$$R''(r) + \frac{1}{r}R' - R + R^3 = 0, \qquad R'(0) = 0, \qquad R(\infty) = 0. \tag{4}$$

Eq. (4) has enumerable number of solutions $\{R^{(n)}\}_{n=0}^{\infty}$, which can be arranged in order of increasing power [4], i.e.,

$$\int (R^{(0)})^2 \,\mathrm{d}x\,\mathrm{d}y \leq \int (R^{(1)})^2 \,\mathrm{d}x\,\mathrm{d}y \leq \int (R^{(2)})^2 \,\mathrm{d}x\,\mathrm{d}y \leq \cdots$$

Of most importance is the ground state solution $R := R^{(0)}$, also known as *Townes profile* [5]. The ground state R is positive and monotonically decreasing. In addition, its power is exactly equal to the critical power N_c, i.e., $N_c = \int R^2 \,\mathrm{d}x\,\mathrm{d}y \approx 11.7$ [6].

The critical NLS (1) is invariant under the lens (pseudo-conformal) transformation, i.e., if ψ is a solution of the NLS (1) then

$$\tilde{\psi} = \frac{1}{L(t)}\psi(\tau,\xi)\exp\left(\mathrm{i}\frac{L_t}{L}\frac{r^2}{4}\right), \qquad r = \sqrt{x^2+y^2}, \qquad \xi = \frac{r}{L(t)}, \qquad \tau = \int_0^t \frac{\mathrm{d}s}{L^2(s)}, \tag{5}$$

where $L(t) = \alpha^2(T_c - t)$, is also a solution of the NLS (1) [7]. Applying the lens transformation (5) to the waveguide solutions $\psi = \mathrm{e}^{\mathrm{i}t}R(r)$ gives rise to the explicit blowup solutions

$$\psi^{\mathrm{ex}}_{R^{(n)}}(t,r) = \frac{1}{L(t)}R^{(n)}\left(\frac{r}{L(t)}\right)\mathrm{e}^{\mathrm{i}\tau+\mathrm{i}(L_t/L)(r^2/4)}, \qquad \tau = \int_0^t \frac{\mathrm{d}s}{L^2(s)}, \qquad L(t) = \alpha^2(T_c - t), \tag{6}$$

where $R^{(n)}$ are the solutions of (4), that become singular at $t = T_c$. These explicit blowup solutions, however, are unstable.

Two related questions which were open from the mid 1960s up to the mid 1980s, were the profile of the solution near the collapse and the rate of blowup. Numerical studies conducted during the 1980s [8,9], suggested that the NLS has a universal, cylindrically-symmetric asymptotic blowup profile

$$\psi \sim \psi_R = \frac{1}{L(t)}R\left(\frac{r}{L(t)}\right)\mathrm{e}^{\mathrm{i}\tau+\mathrm{i}(L_t/L)(r^2/4)}, \qquad \tau = \int_0^t \frac{\mathrm{d}s}{L^2(s)}, \tag{7}$$

where R is the ground-state solution of (4). More precisely, it turned out that only the inner core of the solution collapses into the singularity with the asymptotic profile ψ_R as $t \to T_c$, while the rest of the solution continues to

propagate (see, e.g., Fig. 5), i.e.,

$$\psi \sim \begin{cases} \psi_R & 0 \le r \le \rho L(t) \\ \psi_{\text{outer}} & \rho L(t) < r \end{cases} \tag{8}$$

where $\rho \gg 1$ and $L(t) = 1/\max_{x,y} |\psi(t, x, y)|$. The understanding that NLS collapse is quasi self-similar with asymptotic profile ψ_R was crucial in the asymptotic calculation of the blowup rate $L(t)$, which turned out to be given by the *loglog law* [10–12]

$$L(t) \sim \left(\frac{2\pi(T_c - t)}{\log\log 1/(T_c - t)} \right)^{1/2}, \tag{9}$$

where T_c is the singularity point. Finding the *loglog law* was a hard problem, exactly because the solution undergoes partial beam collapse, in which the inner core evolves according to ψ_R, the outer part propagates linearly, and the dynamics depends on the exponentially weak coupling between the two.

Numerical simulations also showed that ψ_R is an attractor for the inner part of solutions of the weakly perturbed critical NLS. This property was used in the development of an asymptotic theory for the effects of small perturbations in the critical NLS, known as *modulation theory* [1]. Thus, the convergence to ψ_R turned out to be a key feature of the critical NLS. A rigorous proof of the convergence to the self-similar Townes profile ψ_R, however, turned out to be a hard problem. Weinstein proved that near the singularity the solution converges to a self-similar blowup profile [13]. Nawa further characterized the limiting profiles of the collapsing core and of the diffracting outer part [14,15]. These results partially supported the observation that the NLS has the universal asymptotic blowup profile ψ_R, but did not prove it. Only recently, Merle and Raphael proved that solutions of the NLS (1) with power moderately above N_c collapse with the asymptotic profile ψ_R at the loglog blowup rate [16–18]. Concurrently, it was demonstrated experimentally that the profile of collapsing laser beams is given by the Townes profile [19]. Thus, all the research that was carried out from the eighties until these days leads to the belief that the Townes profile is the only attractor of blowup solutions of the critical NLS.

In a recent paper, Bergé et al. presented simulations of the critical NLS with super-Gaussian initial conditions that self-focused with a ring profile [20]. These simulations were only carried out for focusing levels of 3–5, probably because the focus of that paper was on symmetry-breaking (multiple filamentation). In this research, we study such ring-type solutions as they continue to collapse. Specifically, we are interested to know whether the ring structure will persist until the singularity, or whether the solution will eventually collapse with the Townes profile.

The paper is organized as follows. In Section 2 we solve the NLS with high-power super-Gaussian initial conditions and observe numerically that the solution collapses with a quasi self-similar ring profile at a square-root blowup rate up to focusing levels of 10^{16}. In particular, the solution does not change into the Townes profile, nor does it blowup with the loglog blowup rate (9). In Section 3 we find the equation of the ring profile, denoted as the G equation. Section 4 is devoted to analysis of the G equation. We present one-parameter families of ring and multi-ring solutions of the G equation. We then use these solutions to construct explicit self-similar ring solutions of the NLS that blowup at a square root blowup rate. In Section 5 we show numerically that the self-similar profiles of the collapsing ring solutions of the NLS have an excellent match with the single-ring solutions of the G equation. As in the case of the R profile, see Eq. (8), the NLS ring solutions match the G profile only in the "ring region", and not everywhere (i.e., quasi self-similar collapse). In Section 6, we test the stability of the ring profiles and show numerically that the self-similar ring profile is a strong attractor in the radially-symmetric case, but not under symmetry breaking perturbations. We also observe that multi-ring solutions are unstable even in the radially-symmetric case. Section 7 shows that the super-critical NLS also admits collapsing ring solutions, but that they are quite different from the critical NLS ring solutions. In Section 8 we discuss the open question of the existence of H^1 ring-type blowup solutions of the critical NLS. Final remarks are given in Section 9. The numerical methods used in this study are described in the Appendices A–F.

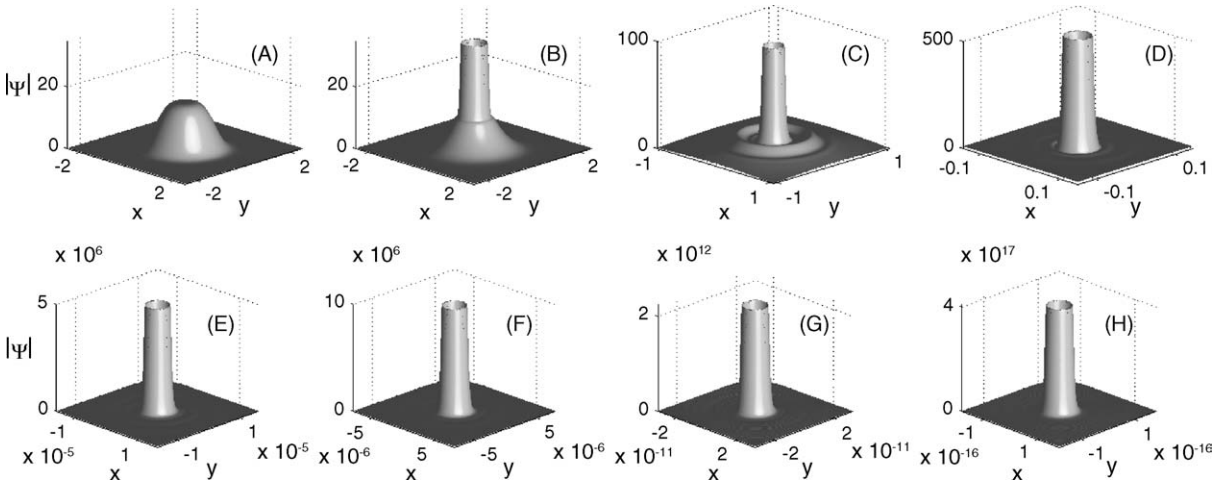

Fig. 1. Solution of the NLS (10) with $\psi_0 = 15\,\mathrm{e}^{-r^4}$. (A) $t = 0$, $A(t) = 1$; (B) $t = 0.020$, $A(t) = 1$; (C) $t = 0.027$, $A(t) = 1$; (D) $t = 0.0286$, $A(t) = 1$; (E) $t = 0.02875793896630$, $A(t) = 3.32 \times 10^5$; (F) $A(t) = 6.64 \times 10^5$; (G) $A(t) = 4.6 \times 10^{10}$; (H) $A(t) = 6.5 \times 10^{15}$. Times t in graph E–H differ only in the 14th digit or after, therefore only the focusing levels $A(t)$ are presented.

2. Preliminary numerical observations

We first ask what happens to ring solutions as they get closer and closer to the singularity (i.e., as they become more and more focused). Specifically, do they maintain a ring profile or does the blowup profile becomes Townesian at a certain stage? To see that, we first solve the radially-symmetric NLS

$$\mathrm{i}\psi_t(t,r) + \psi_{rr} + \frac{1}{r}\psi_r + |\psi|^2\psi = 0, \qquad \psi(0,r) = \psi_0(r), \tag{10}$$

with the high-power super-Gaussian initial condition $\psi_0 = 15\,\mathrm{e}^{-r^4}$ ($N(0) \simeq 38N_c$). In order to be able to get closer and closer to the singularity we use the method of *dynamic rescaling* (see Appendix E). As can be seen in Fig. 1, the solution collapses with a ring profile that becomes taller in amplitude and smaller in radius, up to focusing levels of $A(t) = \mathcal{O}(10^{15})$, where

$$A(t) = \frac{\max_r |\psi(t,r)|}{\max_r |\psi(0,r)|}. \tag{11}$$

In addition, Fig. 1E–H suggest that the ring solution is self-similar, i.e., of the form

$$|\psi(t,r)| \sim \frac{1}{L(t)} G(\xi), \qquad \xi = \frac{r}{L(t)}, \tag{12}$$

for some profile $G(\xi)$. In order to check for self-similarity, we rescale the numerical solution according to[1]

$$\psi_{\text{normalized}}(t,r) = L(t)\psi\left(\frac{r}{L(t)}\right), \qquad L(t) = \frac{1}{\max_r |\psi|}. \tag{13}$$

Fig. 2A shows the results of Fig. 1E–H, rescaled according to (13). All four normalized plots are indistinguishable, indicating that the collapsing ring solution is indeed self-similar while focusing over more than 10 orders of

[1] Note that under the normalization (13), $\max_r |\psi_{\text{normalized}}| = 1$.

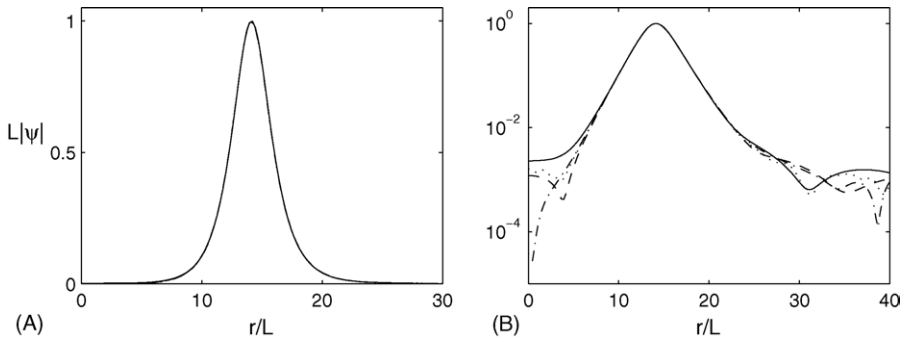

Fig. 2. (A) Results of Fig. 1E–H normalized and superimposed: $A(t) = 3.32 \times 10^5$ (solid), $A(t) = 6.64 \times 10^5$ (dashes), $A(t) = 4.6 \times 10^{10}$ (dots) and $A(t) = 6.5 \times 10^{15}$ (dash-dots); all four lines are indistinguishable. (B) Same data on a semi-logarithmic scale.

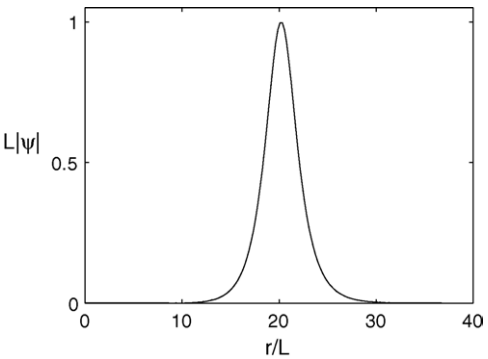

Fig. 3. Solution of the NLS (10) with $\psi_0 = 20\,\mathrm{e}^{-r^4}$ at $t = 0.020793557$ ($A(t) = 1.12 \times 10^3$; solid) and at $t = 0.020793558$ ($A(t) = 1.75 \times 10^5$; dots); the two lines are indistinguishable.

magnitude. Plotting the same data on a semi-logarithmic scale (Fig. 2B) shows that the rescaled profile is only quasi self-similar: it is self-similar in the "ring region", but not near the center ($r/L \ll 10$) or far outside ($r/L \gg 10$).

We now increase the input power and solve the NLS (10) with $\psi_0 = 20\,\mathrm{e}^{-r^4}$ ($N(0) \simeq 67N_c$). In this case the solution also collapses with a self-similar ring profile (Fig. 3). The radius of the rescaled ring in Fig. 3 is $\xi_{\max} \cong 20.2$, which is larger than in Fig. 2 where $\xi_{\max} \cong 14.1$. More generally, we observe that the ring radius increases with the input power. Since different initial conditions collapse with ring structures with different radii, the ring profile appears not to be universal (but see Section 4.2).

In order to show that initial conditions that are different from $\psi_0 = c\,\mathrm{e}^{-r^4}$ can also collapse with a self-similar ring profile, we show in Fig. 4 that the initial condition $\psi_0 = 15\,\mathrm{e}^{-r^8}$ ($N(0) \simeq 43N_c$) also collapses with a self-similar ring profile.[2] Clearly, not all high-power (i.e., $N(0) = \mathcal{O}(50N_c)$) initial conditions collapse with a ring profile. For example, the Gaussian initial condition whose input power is the same as the super-Gaussian $\psi_0 = 15\,\mathrm{e}^{-r^4}$ from Fig. 1, collapses with a Townes profile (see Fig. 5).

We now consider the blowup rate of these ring solutions. Since the solutions were found to be self-similar as in (12), their blowup rate is given by $L(t)$. Plotting L^2 as a function of t looks like a straight line, suggesting an asymptotic square root blowup rate. However, it is hard to determine from such plots whether the blowup rate is strictly a square root or a square root with a small (e.g., *loglog*) correction. A better numerical approach is, therefore,

[2] In Section 6 we show non-monotonic initial conditions that also collapse with a self-similar ring solution.

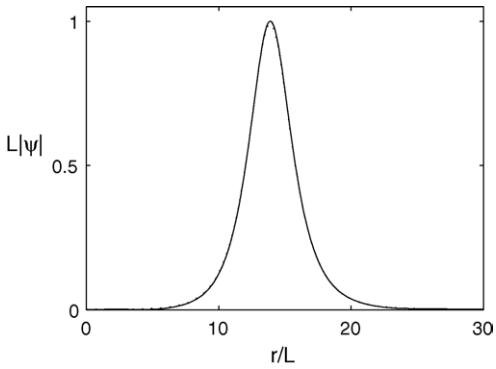

Fig. 4. Solution of the NLS (10) with $\psi_0 = 15\,\mathrm{e}^{-r^8}$, at $t = 0.0302387873$ ($A(t) = 6.625 \times 10^3$; solid) and at $t = 0.0302387878$ ($A(t) = 2.67 \times 10^4$; dots); the two lines are indistinguishable.

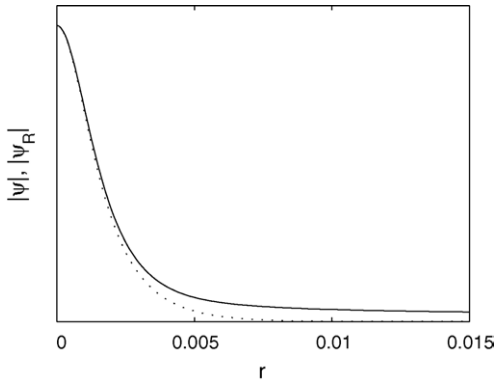

Fig. 5. Solution of the NLS (10) with $\psi_0 = 15\sqrt[4]{\pi/2}\,\mathrm{e}^{-r^2}$ at $t = 0.0172$ (solid). Dotted line is the Townes-based asymptotic profile ψ_R.

to monitor the dynamics of $LL_t = (1/2)(L^2)_t$, since $\lim_{t\to T_c} LL_t = -\alpha^2/2 < 0$ in the case of a strict square root blowup rate $L(t) \sim \alpha\sqrt{T_c - t}$, whereas $\lim_{t\to T_c} LL_t = 0$ when the blowup rate is faster than a square root. Fig. 6A shows that $\lim_{t\to T_c} LL_t \cong 0.085$ for the super-Gaussian initial condition $\psi_0 = 15\,\mathrm{e}^{-r^4}$, suggesting a square root blowup rate of $L(t) \sim \alpha\sqrt{T_c - t}$ with $\alpha \cong 0.41$. Note that this is different from the equal-power Gaussian initial condition from Fig. 5, for which $\lim_{t\to T_c} LL_t = 0$ (see Fig. 6B), which implies a faster-than-a-square-root blowup rate. Therefore, it seems that monitoring LL_t is, indeed, a good way to tell numerically a square root from a faster-than-a-square-root blowup rate.

3. Finding the ring profile $G(\xi)$

The preliminary numerical observations in Section 2 suggest the existence of NLS solutions that collapse with a self-similar ring-profile G at a square-root blowup rate. We now turn our attention to the following question: Which equation describes the ring profile(s)[3] observed in Figs. 2–4? Clearly, G cannot be any of the infinite number of solutions $R^{(n)}$ of Eq. (4), because all these solutions have a global maximum at $r = 0$. Likewise, it cannot be any of

[3] We say profiles and not profile, since they can have different radii.

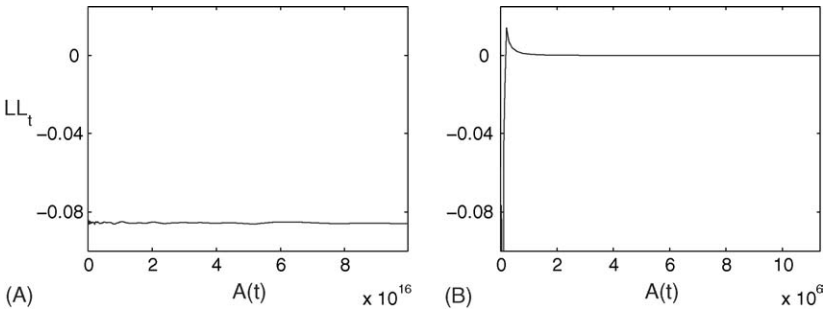

Fig. 6. LL_t as a function of $A(t)$ for solutions of the NLS (10) with initial conditions: (A) $\psi_0 = 15\,\mathrm{e}^{-r^4}$ and (B) $\psi_0 = 15\sqrt[4]{\pi/2}\,\mathrm{e}^{-r^2}$.

the multibump solutions found by Budd [21], since these solutions exist only in the case of the supercritical NLS, (i.e., Eq. (32) for $d > 2$), and even in that case they were found to be numerically unstable.

The following proposition characterizes all singular solutions that undergo self-similar collapse at a square root blowup rate:[4]

Proposition 1. *Let ψ be a singular solution of the NLS (1) with an asymptotic self-similar blowup profile $\psi(t,r) \sim \psi_G(t,r)$ where*

$$\psi_G(t,r) = \frac{1}{L(t)} G(\xi)\,\mathrm{e}^{\mathrm{i}\tau + \mathrm{i}(L_t/L)(r^2/4)}, \qquad \tau = \int_0^t \frac{\mathrm{d}s}{L^2(s)}, \qquad \xi = \frac{r}{L(t)}, \tag{14}$$

and $G(\xi) : \mathbb{R} \to \mathbb{R}$. If ψ has a square root blowup rate, i.e., if

$$\lim_{t\to T_c} \frac{L(t)}{\sqrt{T_c - t}} = \lim_{t\to T_c} \frac{\mathrm{d}(L(t))/\mathrm{d}t}{\mathrm{d}(\sqrt{T_c - t})/\mathrm{d}t} = \alpha > 0, \tag{15}$$

then $G(\xi)$ is the solution of

$$G''(\xi) + \frac{G'}{\xi} + \left[\frac{\alpha^4}{16}\xi^2 - 1\right] G + G^3 = 0, \qquad 0 \neq G(0) \in \mathbb{R}, \qquad G'(0) = 0. \tag{16}$$

Proof. Substitution of (14) in the NLS (1) shows that the equation for G is

$$G''(\xi) + \frac{G'}{\xi} - G + G^3 + \frac{1}{4}\beta(t)\xi^2 G = 0, \qquad \beta(t) = -L_{tt}L^3. \tag{17}$$

Since $G(\xi)$ is independent of t, $\beta(t) \equiv \beta_0 := \beta(0)$. Hence, the equation for $L(t)$ is

$$L_{tt} = -\frac{\beta_0}{L^3}.$$

Multiplying this equation by L_t and integrating gives,

$$(LL_t)^2 = \beta_0 + C_0 L^2, \qquad C_0 = L_t^2(0) - \frac{\beta_0}{L^2(0)}.$$

[4] A "modified" version of Proposition 1 for quasi self-similar collapse is given in Section 8.

Therefore, since $\lim_{t\to T_c} L(t) = 0$,

$$\lim_{t\to T_c} (LL_t)^2 = \beta_0 + \lim_{t\to T_c} C_0 L^2 = \beta_0. \tag{18}$$

When the blowup rate is a square root, it follows from (15) that

$$\lim_{t\to T_c} LL_t = -\frac{\alpha^2}{2}. \tag{19}$$

Therefore, by (18) and (19),

$$\beta_0 = \frac{\alpha^4}{4}. \tag{20}$$

Substituting (20) into (17) gives (16). □

We, therefore, see that the profile of self-similar solutions that blowup at a square root rate is given by the G Eq. (16), and not by the R Eq. (4). In Section 4 we will show that solutions of Eq. (16) can, indeed, give rise to ring solutions and in Section 5.2 we will show that the G-profiles provide an excellent match to the ring solutions observed in the simulations of Section 2.

Remark 2. Eq. (16) is not new. In fact, it frequently arises in the analysis of blow-up solutions of the NLS. Until now, however, this equation was analyzed by assuming that to leading order, this equation reduces to the R-profile (4). Therefore, it was assumed that $G(0) = R(0) + \mathcal{O}(\alpha^4) = \mathcal{O}(1)$. In contrast, in this study we are interested in solutions of Eq. (16) with $G(0) \ll 1$ that give rise to ring solutions.[5]

It is generally hard in NLS simulations to characterize the small derivation (if any) from a square root blowup rate, even in simulations where the solution focuses by 10^{15}. As we have seen in Fig. 6, monitoring the dynamics of LL_t seems to provide a good way to distinguish between a strict square root blowup rate and a faster-than-a-square-root blowup rate. Although Fig. 6 provides a strong numerical support that the ring self-similar solution collapses with a square root blowup rate, the numerical data cannot determine in a conclusive manner whether the blowup rate is exactly a square root. Therefore, we ask whether is it possible that NLS solutions with a self-similar ring profile collapse at a different blowup rate. Since the blowup rate has the rigorous bound $L(t) \le M\sqrt{T_c - t}$ where M is a constant [22,23], we need to consider only the case where the blowup rate is faster than a square root, i.e., when $\lim_{t\to T_c} LL_t = 0$ (see Section 2). This is done in the following proposition:

Proposition 3. *Let ψ be a solution of the NLS (1) with an asymptotic self-similar blowup profile (14). If the blowup rate of ψ is faster than a square root, i.e., if*

$$\lim_{t\to T_c} LL_t = 0, \tag{21}$$

then, $G(\xi)$ is the solution of the R Eq. (4).

Proof. From (18) and (21), it follows that $\beta_0 = 0$. Substituting this results in (17) gives the R Eq. (4). □

Remark 4. Proposition 3 applies to the case of loglog blowup rate (9), as well as to the linear blowup rate $L(t) = \alpha(T_c - t)$ of the explicit blowup solutions $\psi_{ex}^{(n)}$ of (6).

[5] Indeed, since $G''(0) = G(0)(1 - G^2(0))/2$, G is increasing at $\xi = 0$ if and only if $G(0) < 1$.

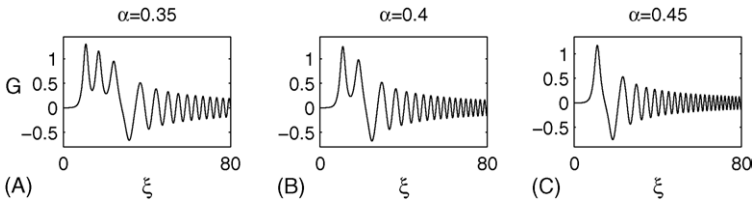

Fig. 7. Solutions of Eq. (16) with $G_0 = 5 \times 10^{-4}$ for several values of α.

4. Ring solutions of the G equation

Solutions of the G Eq. (16) depend on the parameter α and on the initial condition $G_0 = G(\xi = 0)$. Let us recall Theorem 1.1 of [24] of Johnson and Pan, applied here to Eq. (16):

Lemma 5. *All solutions of the initial value problem (16) are decaying as $\xi \to \infty$. Moreover,*

$$G(\xi) = \frac{c_G}{\xi} \cos\left(\frac{\alpha^2}{8}\xi^2 - \frac{2}{\alpha^2}\log\xi + c_2\right) + \mathcal{O}\left(\frac{1}{\xi^2}\right), \tag{22}$$

where c_G and c_2 are constants that depend on G_0 and on α.

Lemma 5 ensures that for any G_0 (and for any α) the solution decays as $\xi \to \infty$. This is different from the case of the R Eq. (4), where decaying solutions exist only for enumerable set of values of $R(0)$, see [4].

4.1. Families of n-ring profiles

As we have mentioned, we are interested in solutions of Eq. (16) with $G_0 \ll 1$ that give rise to ring-type solutions. Fig. 7 shows solutions of Eq. (16) with $G_0 = 5 \times 10^{-4}$ for various values of α. In general, these solutions can be separated into two regions:

(1) A ring region for $0 \le \xi \le \mathcal{O}(1/\alpha^2)$, in which G is positive with one or several rings.
(2) A tail of decaying-to-zero oscillations for $\xi \gg 1/\alpha^2$ (see Lemma 5).

Clearly, we are interested in solutions of the G equation that look as in Figs. 2–4 and not as in Fig. 7, i.e., without the oscillatory tail. Since the amplitude of the decaying oscillations is governed by c_G, see Eq. (22), we can equivalently say that we are interested in ring solutions of Eq. (16) with the smallest-possible tail (i.e., c_G).[6] Therefore, for a given G_0, we can define the single-ring profile of Eq. (16) as the single-ring solution with the value of α that gives rise to the smallest-possible c_G. More generally, the n-ring profile is the n-ring solution with the minimal c_G.[7] Fig. 8 shows a graph of c_G as a function of α for $G_0 = 5 \times 10^{-4}$ (see Appendix B for numerical methods to calculate c_G). In general c_G is $\mathcal{O}(10)$, but it sharply falls into minimum points at several locations. Let us denote the values of α at the minimum points by, going from left to right, $\alpha^{(1)}, \alpha^{(2)}, \alpha^{(3)}, \ldots$. Plotting the corresponding G-profiles shows that $\alpha = \alpha^{(n)}$ corresponds to an n-ring profile (see Fig. 9). The sharp variation of c_G near the minima points in Fig. 8 indicates that slight perturbations in the value of α from $\alpha^{(n)}$ result in solutions which are very different

[6] See also discussion in Section 9.
[7] The minimum value of c_G is close to, but not equal to, zero (see Fig. 8). Indeed, from Lemma 5 it follows that if $c_G = 0$ then $G \equiv 0$. Therefore, an n-ring solution of (16) does have an oscillating tail, but its magnitude is minimal.

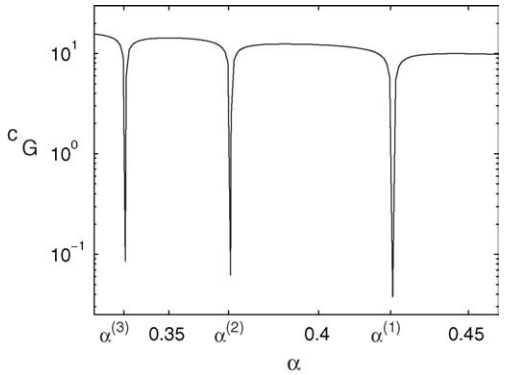

Fig. 8. Graph of c_G as a function of α for $G_0 = 5 \times 10^{-4}$.

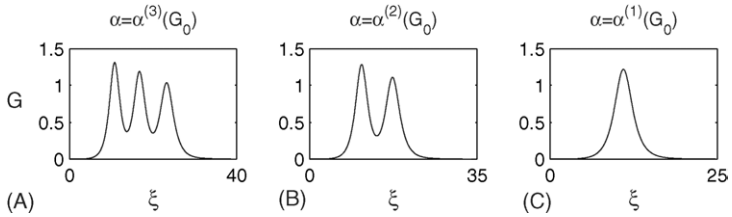

Fig. 9. Solutions of Eq. (16) with $G_0 = 5 \times 10^{-4}$ and (A) $\alpha = \alpha^{(3)}(G_0) \cong 0.0335$, (B) $\alpha = \alpha^{(2)}(G_0) \cong 0.37$ and (C) $\alpha = \alpha^{(1)}(G_0) \cong 0.424$.

from ring profiles (see Fig. 10). More generally, values of α between $\alpha^n < \alpha < \alpha^{n+1}$ give rise to n-ring solutions with "large" oscillating tails (as in, e.g., Fig. 7).

Let us denote by $\alpha^{(n)}(G_0)$ the value of α for which the solution of Eq. (16) with the initial condition $G(0) = G_0$ is an n-ring profile, according to the above definition of ring profiles, i.e., $\alpha^{(n)}(G_0)$ is a minimum point of the graph $c_G(\alpha)$. By repeating the above process for other values of G_0 (namely calculating c_G as a function of α and finding the minimum points $\alpha^{(n)}$, see Appendix B for more details), we can obtain curves $\alpha = \alpha^{(n)}(G_0)$

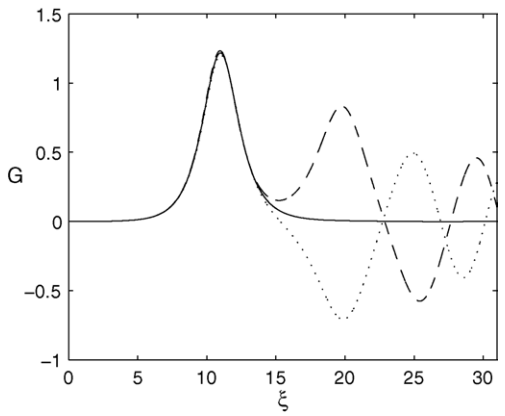

Fig. 10. Solutions of Eq. (16) with $G_0 = 5 \times 10^{-4}$ and $a = \alpha^{(1)}$ (solid), $\alpha = \alpha^{(1)} + 0.01$ (dotted) and $\alpha = \alpha^{(1)} - 0.01$ (dashed).

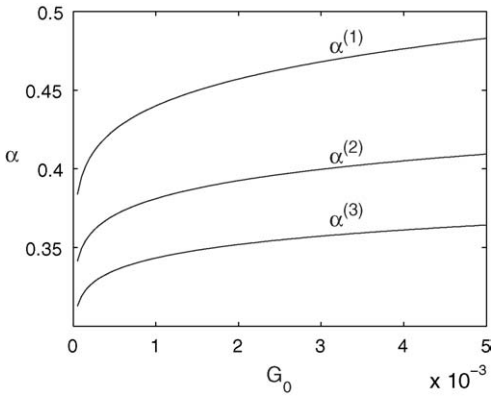

Fig. 11. The curves $\alpha^{(n)}(G_0)$ that corresponds to n-ring profile solutions of Eq. (16).

that describe families of n-ring profiles (see Fig. 11). As we have pointed out earlier, values of α between the curves $\alpha^{(n)}(G_0) < \alpha < \alpha^{(n+1)}(G_0)$, correspond to n-ring solutions with a non-small oscillating tail.

Remark 6. As we have just seen, in the case of ring solutions of the critical NLS,α can assume a continuous range of values. In contrast, α has to be equal to zero in the case of Townesian blowup solution of the critical NLS, and in the case of the super-critical NLS the value of α can assume a single value (e.g., $\alpha \cong 0.9177$ when $d = 3$ in Eq. (32)) [9].

4.2. *"Universality" of the G-profile*

In Section 2 we concluded that the G-profile is not universal since different initial condition evolve into rings of different radii.

In Section 4 we have also seen that the value of α is also not universal.

We now consider the behavior of the G-profile around its peak(s):

Lemma 7. *Let G be a solution of* Eq. (16) *and let $\xi_{\max}$ be a local maximum point of G such that*

$$1 \ll \xi_{max} \leq \frac{4}{\alpha^2}. \tag{23}$$

Then for $|\xi - \xi_{\max}| = \mathcal{O}(1)$,

$$G(\xi) \sim \nu \operatorname{sech}\left(\nu \frac{\xi - \xi_{\max}}{\sqrt{2}}\right), \qquad \nu^2 = 2 - \frac{\alpha^4}{8}\xi_{\max}^2. \tag{24}$$

Proof. Since $G'(\xi_{\max}) = 0$ and $\xi \gg 1$, the term $G'(\xi)/\xi$ can be neglected. In addition, since $\xi \gg 1$ and $|\xi - \xi_{\max}| = \mathcal{O}(1)$, it follows that $\xi^2 = \xi_{\max}^2(1 + o(1))$. Hence, to leading order Eq. (16) reduces to

$$G''(\xi) + \left[\frac{\alpha^4}{16}\xi_{\max}^2 - 1\right] G + G^3 = 0, \qquad G'(\xi_{\max}) = 0, \tag{25}$$

whose solution is given by (24). □

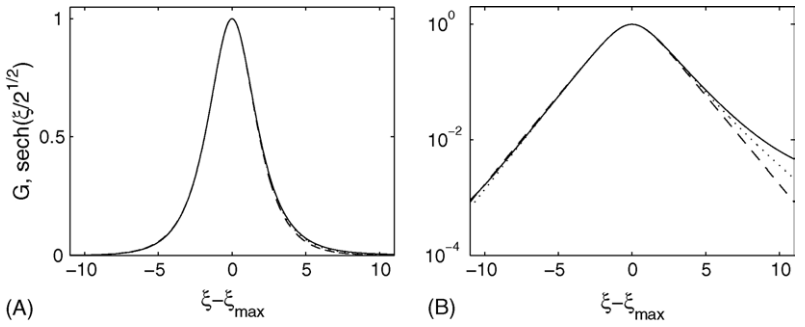

Fig. 12. (A) Single ring G-profiles with $G_0 = 5 \times 10^{-4}$ and $\alpha = \alpha^{(1)} \cong 0.424$ (solid) and with $G_0 = 7.6 \times 10^{-6}$ and $\alpha = \alpha^{(1)} \cong 0.357$ (dots). Also plotted is $\mathrm{sech}(\xi/\sqrt{2})$ (dashes). (B) Same data on a semi-logarithmic scale.

Remark 8. Condition (23) ensures that $\xi_{\max}$ is in the ring region, and not in the oscillatory tail.

Remark 9. In the case of multi-ring solutions, Lemma 7 applies to each peak of the rings.

Lemma 7 shows that up to radial translations and dilations, all ring solutions have the same profile in the ring region, which is given by the well-known one-dimensional sech soliton. To illustrate that, we plot in Fig. 12A the single-ring solutions of Eq. (16) with $G_0 = 5 \times 10^{-4}$ and with $G_0 = 7.6 \times 10^{-6}$ rescaled according to (13) and centered around their corresponding peaks (at $\xi_{\max} \cong 10.98$ and $\xi_{\max} \cong 15.54$, respectively), together with a plot of $\mathrm{sech}(\xi/\sqrt{2})$. As predicted by Lemma 7, there is an almost perfect match between the two single-ring G-profiles and the sech profile. More precisely, the match is excellent near the peak ($|\xi - \xi_{\max}| \leq 3$); for $3 \leq \xi - \xi_{\max} \leq 10$ the G-profile lies slightly above the sech profile (see Fig. 12B). Based on Lemma 7 and the results shown in Fig. 12 we can say that, in a sense, the G-profile is after all universal.

4.3. Self-similar ring collapse—explicit solutions

We can construct explicit self-similar ring blowup solutions by substituting $L = \alpha\sqrt{T_c - t}$ in the asymptotic profile ψ_G (14):

Lemma 10. *Let*

$$\psi_G^{(\mathrm{ex})} = \frac{1}{\alpha\sqrt{T_c - t}} G\left(\frac{r}{\alpha\sqrt{T_c - t}}\right) \mathrm{e}^{-\mathrm{i}((\log(T_c - t))/\alpha^2) - \mathrm{i}(r^2/8(T_c - t))}, \tag{26}$$

where $G(\xi;\alpha)$ is a solution of (16). Then, ψ_G is an explicit blowup solution of the NLS whose blowup rate is $L(t) = \alpha\sqrt{T_c - t}$.

Proof. A straightforward substitution of ψ_G (26) into the NLS (1) proves the result. □

Remark 11. Lemma 10 applies to any solution of (16), and not just to n-ring G-profiles where $\alpha = \alpha^{(n)}$.

Lemma 5 implies that G (and hence ψ_G) have infinite L^2 norms. Therefore, Lemma 10 proves the existence of collapsing self-similar ring solutions of the NLS that blowup at a square root blowup rate which are not in H^1. Existence of H^1 ring type blowup solutions is discussed in Section 8.

5. NLS simulations of collapsing ring solutions

5.1. Explicit single-ring blowup solution

In order to reproduce numerically the explicit single-ring blowup solution $\psi_G^{(\mathrm{ex})}$, we first derive a simpler form of (26). To do that, let

$$\tilde{\psi}_G^{(\mathrm{ex})} = \mathrm{e}^{\mathrm{i}((\log(T_c-\alpha^2 T_c t)/\alpha^2)/\alpha^2)}\lambda\psi_G(\lambda^2 t, \lambda r), \qquad \lambda = \alpha\sqrt{T_c}.$$

Dropping the tilde, we obtain that

$$\psi_G^{(\mathrm{ex})}(t, r) = \frac{1}{\sqrt{1-\alpha^2 t}} G\left(\frac{r}{\sqrt{1-\alpha^2 t}}\right) \mathrm{e}^{-\mathrm{i}(\alpha^2 r^2/8(1-a^2 t))}, \tag{27}$$

is an explicit blowup solution of the NLS with a square root blowup rate that blows up at $T_c = 1/\alpha^2$. Setting $t = 0$ in (27) we obtain the corresponding initial condition

$$\psi_G^0 = G(r)\,\mathrm{e}^{-\mathrm{i}(\alpha^2/8)r^2}. \tag{28}$$

We solve the NLS (10) with the initial condition ψ_G^0 from (28), with $G_0 = 7.6 \times 10^{-6}$ and $\alpha = \alpha^{(1)}(G_0) \cong 0.357$. The corresponding NLS analytical solution is, of course, given by ψ_G of (27). Fig. 13A shows that, as expected, the numerical solution collapses with a ring profile. Since the normalized solution remains unchanged while focusing by a factor of 10^{15} (Fig. 13B), the solution indeed undergoes self-similar collapse. Moreover, Fig. 14 shows that the blowup rate of the solution is a square root. The graph of LL_t is much smoother than in Fig. 6A, since in the case of ψ_G, $L(t) \equiv \alpha\sqrt{T_c - t}$.

The purpose of this simulation was not to find the solution (which is known analytically), but rather to serve as a benchmark for other simulations. In addition, the fact that the solution maintained a self-similar profile while focusing over 15 orders of magnitude suggests that the self-similar G-profile is stable, as will be further shown in Section 6.1.1.

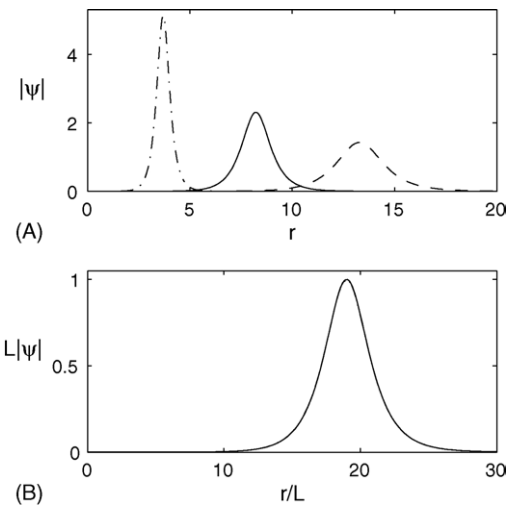

Fig. 13. (A) Solution of the NLS (10) with initial condition ψ_G^0 at $t = 2.103$ (dashes), $t = 5.629$ (solid) and $t = 7.376$ (dash-dots). (B) The three lines from A (at focusing levels $A(t) = 1.17, 1.89, 4.2$) normalized according to (13). Also plotted is the solution at focusing levels of $A(t) = 2.22 \times 10^8$ (dots) and $A(t) = 3.48 \times 10^{15}$ (dash-dots). All five lines are indistinguishable.

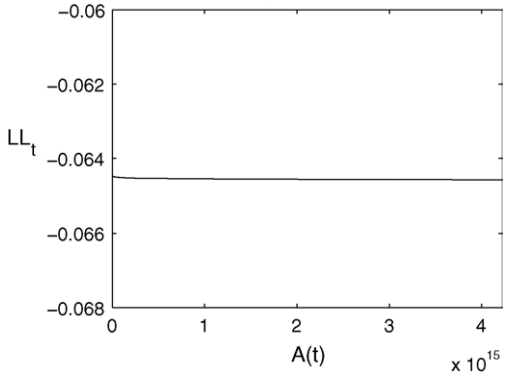

Fig. 14. Blowup rate of the solution of the NLS (10) with $\psi_0 = \psi_G^0$.

5.2. Matching NLS ring solutions with the G-profile

In Figs. 2–4 we showed NLS solutions with high-power super-Gaussian initial conditions that collapsed with a self-similar ring profile. Fig. 15A–C shows that these self-similar profiles have an almost perfect match with the single ring G-profiles that have the same radii (see Appendix D for numerical details on how to match with a G-profile).

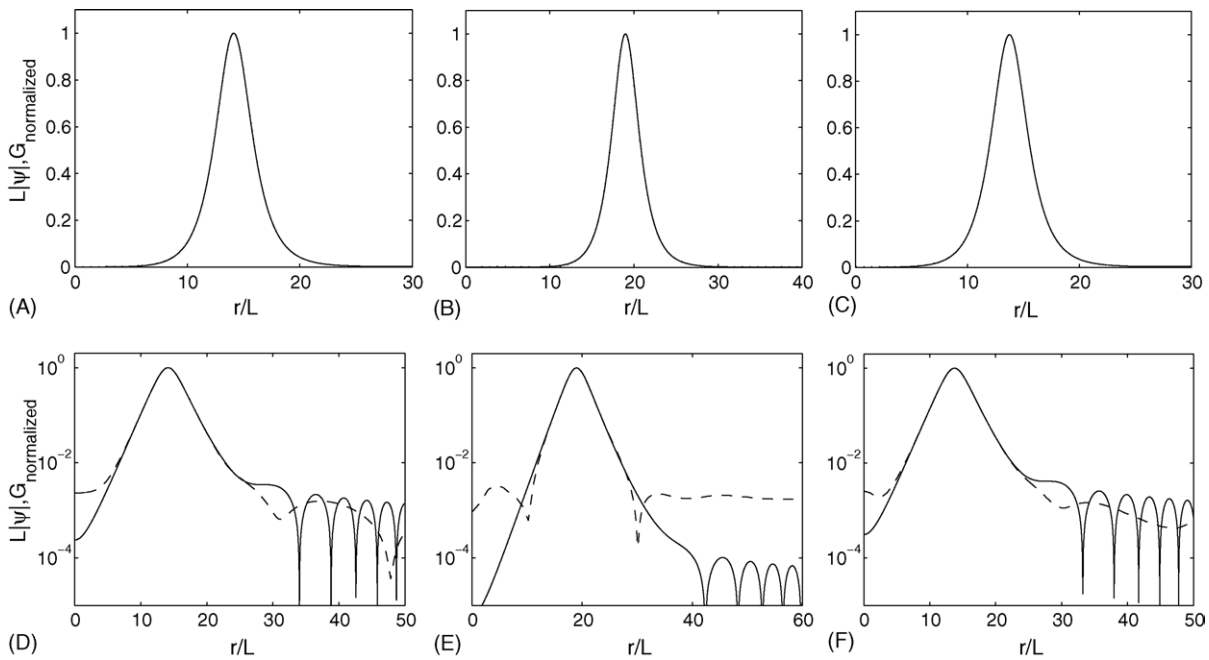

Fig. 15. Solutions of NLS (10) (dashes) and the best fitted G-profile (solid) normalized according to (13). (A) $\psi_0 = 15\,\mathrm{e}^{-r^4}$, normalized profile of ψ at $A(t) = 6.5 \times 10^{15}$, G-profile with $G_0 = 0.000288$ and $\alpha = \alpha^{(1)}(G_0) \cong 0.413$; the two lines are indistinguishable. (B) Same as A with $\psi_0 = 20\,\mathrm{e}^{-r^4}$, $A(t) = 1.75 \times 10^5$, $G_0 = 7.6 \times 10^{-6}$ and $\alpha = \alpha^{(1)}(G_0) \cong 0.357$. (C) Same as A with $\psi_0 = 15\,\mathrm{e}^{-r^8}$, $A(t) = 2.67 \times 10^4$, $G_0 = 0.00038053$ and $\alpha = \alpha^{(1)}(G_0) \cong 0.419$. (D–F) Same data as on top, but on a semi-logarithmic scale.

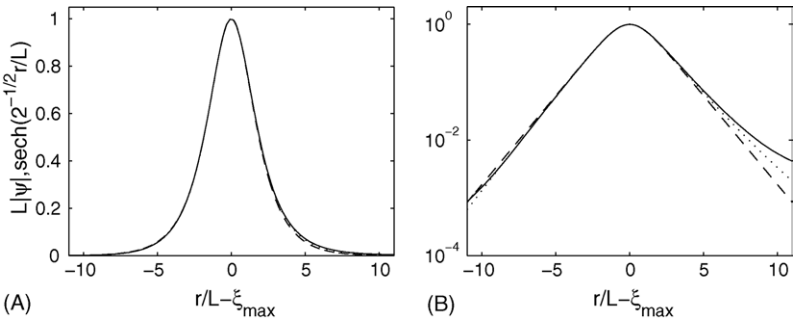

Fig. 16. (A) Self-similar ring profiles of Fig. 15: $\psi_0 = 15\,\mathrm{e}^{-r^4}$ (solid), $\psi_0 = 20\,\mathrm{e}^{-r^4}$ (dotted) and $\psi_0 = 15\,\mathrm{e}^{-r^8}$ (dash-dotted). All three lines are nearly indistinguishable. Dashed line is $\mathrm{sech}(\xi/\sqrt{2})$. (B) Same data on a semi-logarithmic scale.

Remark 12. Under the above matching approach, the value of α (hence of G(0)) is found by looking for a G-profile that has the same radius as the ring solution. For example, for the super-Gaussian initial condition $\psi_0 = 15\,\mathrm{e}^{-r^4}$, we obtain $\alpha = \alpha^{(1)}(G_0) \cong 0.413$. The value of α can be independently extracted from the numerical data using the relation $\lim_{t\to T_c} LL_t = -\alpha^2/2$, see (19). For example, $\lim_{t\to T_c} LL_t \cong 0.085$ for the super-Gaussian initial condition $\psi_0 = 15\,\mathrm{e}^{-r^4}$, see Fig. 6A, yielding $\alpha \cong 0.412$. The fact that we recover nearly the same value of α using two different methods provides an additional support for the validity of the asymptotic ansatz (14)–(16).

Plotting the data of Fig. 15A–C on a semi-logarithmic scale (Fig. 15D–F) shows that the G-profiles provide an excellent match for the self-similar profiles around the ring, but behaves very differently when $\xi = \mathcal{O}(1)$ and when $\xi \gg 1/\alpha^2$. This "mismatch" is expected, since the NLS solutions themselves maintain a self-similar profile only around the ring (see Fig. 2B).

When the three ring profiles from Fig. 15 are plotted as a function of the radial distance from their corresponding peaks (see Fig. 16), we observe that all three ring profiles are almost indistinguishable. This "universality" was predicted by Lemma 7 which states that all (normalized) ring profiles behave like $\mathrm{sech}(\xi/\sqrt{2})$. Indeed, the graph of $\mathrm{sech}(\xi/\sqrt{2})$ agrees very well with these three profiles. The agreement is excellent near the peak ($|\xi - \xi_{\max}| \le 3$); for $3 \le \xi - \xi_{\max} \le 10$, the NLS ring profile lies slightly above the sech profile. Comparison of Fig. 16B with Fig. 12B thus shows that the G-profile does not only "capture" the agreement of the NLS ring solutions with the universal sech profile near the peak, but also the small positive difference from the sech profile for $3 \le \xi - \xi_{\max} \le 10$.

5.3. *"Low power" initial conditions*

In Section 2 we saw that solutions of the NLS (10) with high-power ($N(0) = \mathcal{O}(50N_c)$) super-Gaussian initial condition collapsed with a self-similar ring profile. On the other end, Merle and Raphael [16–18] proved that there exists an universal constant α^*, such that all singular solutions of the NLS (1) whose power is less than $N_c + \alpha^*$ collapse with the ψ_R profile. While the studies [16–18] do not provide the value of α^*, a simple bound for α^* can be obtained by calculating the power of the first excited state explicit solution $\psi^{\mathrm{ex}}_{R^{(1)}}$, see Eq. (6), which clearly does not blowup with the ψ_R profile. Since, $\|\psi^{\mathrm{ex}}_{R^{(1)}}\|_2^2 = \|R^{(1)}\|_2^2 \cong 6.6N_c$, we obtain the bound $\alpha^* \le 5.6N_c$. Therefore, since the rings that we observe are at powers that are of $\mathcal{O}(50N_c)$, there is no contradiction between our observations and the results of Merle and Raphael.

The results of Merle and Raphael imply that ring-type blowup can only occur above a certain power threshold. We now ask what is the minimal power threshold necessary for solutions to collapse with a ring profile. In order to answer this question, we first study a borderline case (see Figs. 17 and 18) of the super-Gaussian initial solution

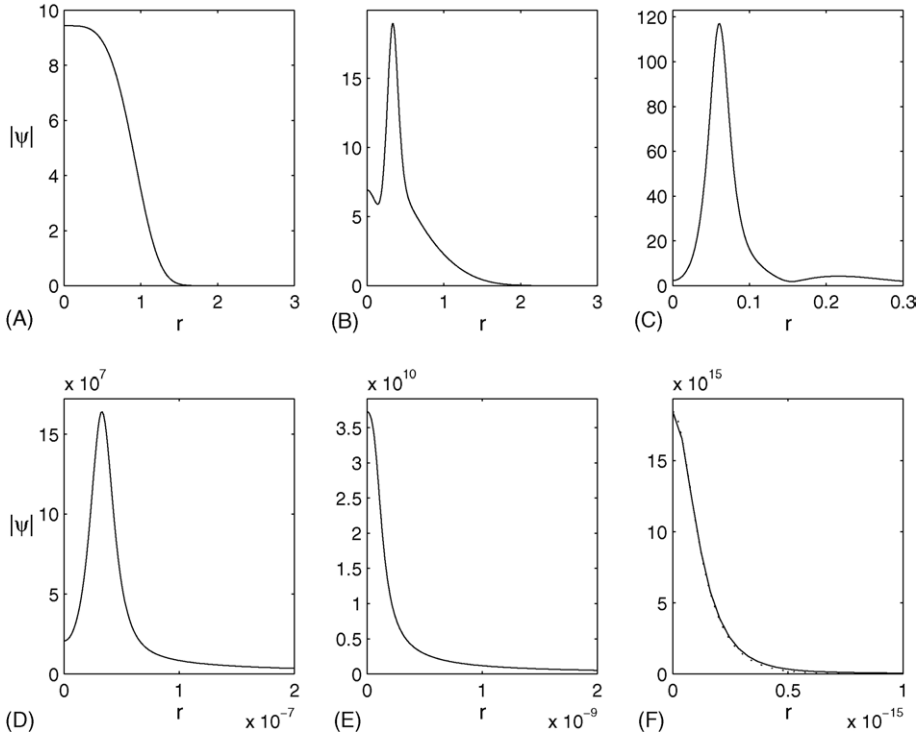

Fig. 17. Solution of the NLS (10) with initial condition power $\psi_0 = \sqrt{60N_c/\pi}\,e^{-r^4}$ with $N(0) = 15N_c$. (A) $t = 0$, $A(t) = 1$, (B) $t = 0.035$, $A(t) = 2$, (C) $t = 0.0485$, $A(t) = 12.4$, (D) $t = 0.04887767073216617$, $A(t) = 1.73 \times 10^7$, (E) $t = 0.0488776707321662$, $A(t) = 4.01 \times 10^9$, (F) $A(t) = 1.95 \times 10^{15}$. Dotted line in F is the rescaled Townes profile R.

$\psi_0 = c\,e^{-r^4}$ with $N(0) = 15N_c (c \cong 9.44)$. Initially, the solution collapses with a ring-like profile that persists up to a focusing level of $A(t) = 10^7$ (B–D). However, at a later stage the relative magnitude of the on-axis amplitude $|\psi(t, r = 0)|$ becomes larger and larger until the global maximum is obtained at the origin (E), so that eventually it collapses with a Townes profile (F).

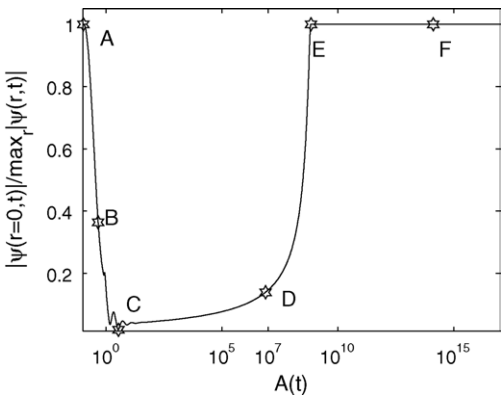

Fig. 18. Relative magnitude at the origin, as a function of the focusing level $A(t)$ for the simulation of Fig. 17. Annotations A–F correspond to graphs A–F in Fig. 17.

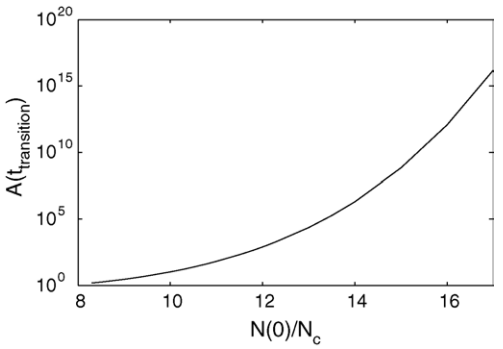

Fig. 19. Focusing level $A(t)$, at time of transition from a ring profile to a Townes profile. The initial conditions are $\psi_0 = c\,\mathrm{e}^{-r^4}$.

In order to study the dependence of the transition from a ring to Townes profile on the input power, we need to define the "*transition time*". A possible definition for the "*transition time*" of the solution from a ring profile to Townes profile is the time when the solution attains its maximum at the origin for the first time since $r \neq 0$, i.e.,

$$t_{\text{transition}} = \inf_{t>0} \left\{ \frac{|\psi(t,0)|}{\max_r |\psi(t,r)|} = 1 \right\}. \tag{29}$$

For example, for the simulation of Fig. 17, the transition occurs at annotation E in Fig. 18. For $N(0) < 10N_c$ the transition occurs during the early stages of the collapse, i.e., for $A(t_{\text{transition}}) = \mathcal{O}(1)$ (see Fig. 19). However, when $N(0) > 10N_c$, the focusing level of the solution at the transition point grows at a super-exponential rate as a function of initial power, and reaches $A(t_{\text{transition}}) = 10^{16}$ when $N(0) = 17N_c$. Since our numerical code may become unreliable at focusing levels above 10^{16}, we cannot determine numerically whether such a transition will occur at much higher powers.[8]

6. Stability of ring profiles

6.1. Radially-symmetric case

We now test the stability of collapsing self-similar ring solutions of the radially-symmetric NLS (10). Clearly, in this case, all perturbations preserve the radial symmetry.

6.1.1. Stability of ring profiles

In Fig. 13 we solved the NLS (10) with initial condition ψ_G^0, whose analytical solution is given by ψ_G. The fact that in the simulation the solution remained self-similar while focusing by a factor of 10^{15} suggests that the self-similar ring profile ψ_G is stable despite the presence of numerical noise. To further test the stability of ψ_G, we randomly perturbed the initial ring profile from Fig. 13 as follows,

$$\psi_0^{\text{noise}} = (1 + \varepsilon_1(r))\psi_G^0 + \varepsilon_2(r), \tag{30}$$

where $\varepsilon_1(r)$ and $\varepsilon_2(r)$ are uniformly distributed in $[-0.25, 0.25]$ and in $[-0.05, 0.05]$, respectively. Note that for this initial condition both the ring and the inner and outer regions are perturbed (see Fig. 20A). After focusing by less than 2, the noise in ring region (i.e., the area of high nonlinearity) has disappeared (Fig. 20B). Then, the noise at

[8] See also discussion in Section 9.

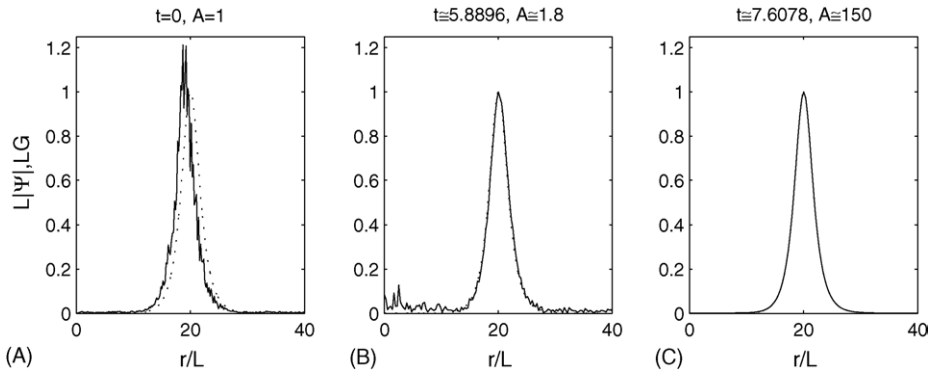

Fig. 20. Solution of the NLS (10) with the noisy initial condition (30); solid line. Dotted line is the G-profile with $G_0 = 3.5 \times 10^{-6}$.

the inner and outer regions slowly decreases, until after focusing by a factor of 150, the solution approaches a clean ring profile. We, therefore, conclude that the self-similar ψ_G profile is a strong attractor in the radially-symmetric case.

Notice that in the absence of noise, the radius of the initial G-profile is $\xi_{\max} = 18.99$ (see Fig. 13B). However, when noise is added, the solution approaches a different G-profile with a larger radius ($\xi_{\max} = 20.05$). The reason for the increase in the radius is that the noise that was added to ψ_G^0 increased the initial power from $N(\psi_G^0) \approx 29N_c$ to $N(\psi_0^{\text{noise}}) \approx 31N_c$.

6.1.2. *Stability of multi-ring profiles*

We now test the stability of the collapsing self-similar solutions ψ_G, in which G is a multi-ring profile. To do that, in Figs. 21 and 22 we solve the NLS (10) with the initial condition ψ_G^0 of (28), where G is the solution of Eq. (16) with the parameters $G_0 = 0.00005$ and $\alpha = \alpha^{(2)}(G_0) \cong 0.37$ (double-ring profile) and $\alpha = \alpha^{(3)}(G_0) \cong 0.335$ (triple-ring profile). In both cases, initially the numerical solution remains close to the analytical solution ψ_G, i.e., all the

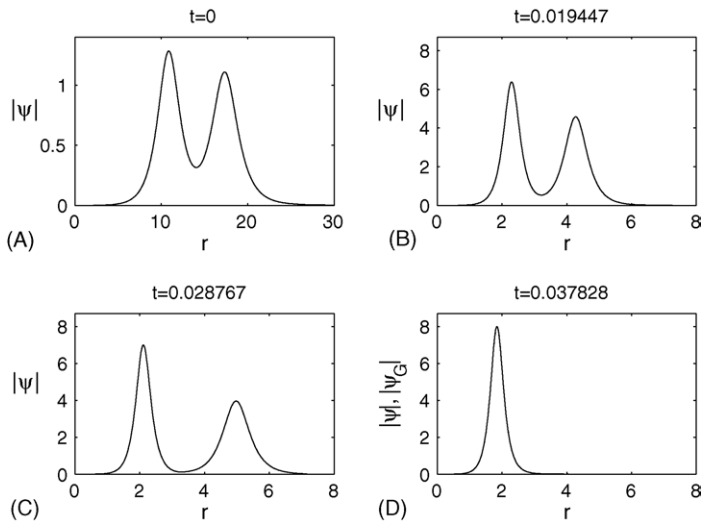

Fig. 21. Dynamics of double-ring solution (solid). Dotted line in D is the best-fitting single ring profile ψ_G; the two lines are indistinguishable.

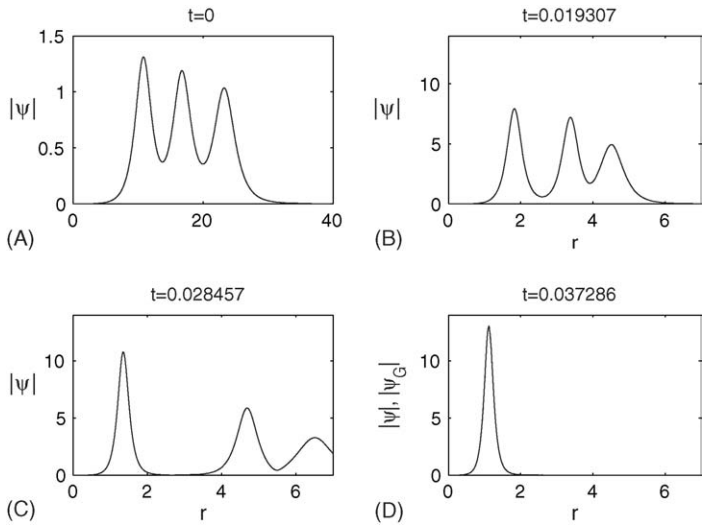

Fig. 22. Dynamics of triple-ring solution (solid). Dotted line in D is the best-fitting single ring profile; the two lines are indistinguishable.

rings collapse towards the center at the same rate. However, after focusing by a factor of 5, the outer ring(s) begin to diffract, i.e., become wider and less focused. Hence, the outer ring(s) move away from the inner ring that continues to collapse. We note that in the simulation of Figs. 21 and 22 we use the same numerical parameters (grid resolution, etc.) as in the benchmark simulation in Fig. 13 which maintained the self-similar profile after focusing by a factor of 10^{15}. Therefore, we conclude that multi-ring solutions are unstable.

Inspection of the collapsing inner ring shows that it approaches a single ring profile (Figs. 21D and 22D). This shows that the single-ring profile ψ_G is an attractor not only for initial conditions of the form $\psi_0 = c\,\mathrm{e}^{-r^{2n}}$ and even not only for monotonically decreasing initial conditions.

6.2. Anisotropic case

We now present numerical simulations of collapsing ring solutions of the NLS (1). Solving (1) numerically is much more demanding than solving (10) and was done using the iterative grid redistribution (IGR) (see Appendix F). We use these simulations to study the effect of breakup of radial-symmetry on collapsing ring solutions. In order to be able to conduct grid convergence testing, we use a deterministic breakup of radial-symmetry (elliptic initial conditions) rather than "count" on symmetry breaking due to numerical noise.

6.2.1. Explicit single-ring initial conditions

Our simulations in Section 6.1.1 show that the collapsing self-similar single ring profile is stable in the radially symmetric case. We now test the stability of ring solutions in the anisotropic case, in which symmetry breaking is due to the introduction of small ellipticity in the initial condition. Ideally, we would like to solve the NLS (1) with the elliptic ring initial condition

$$\psi_0(x, y) = \psi_G^0\left(r = \sqrt{x^2 + (1+\varepsilon)y^2}\right).$$

However, even with the iterative grid redistribution method (see Appendix F), this simulation seems to be too demanding at present. Therefore, we first solve the radially-symmetric NLS (10) with the ring initial condition ψ_G^0

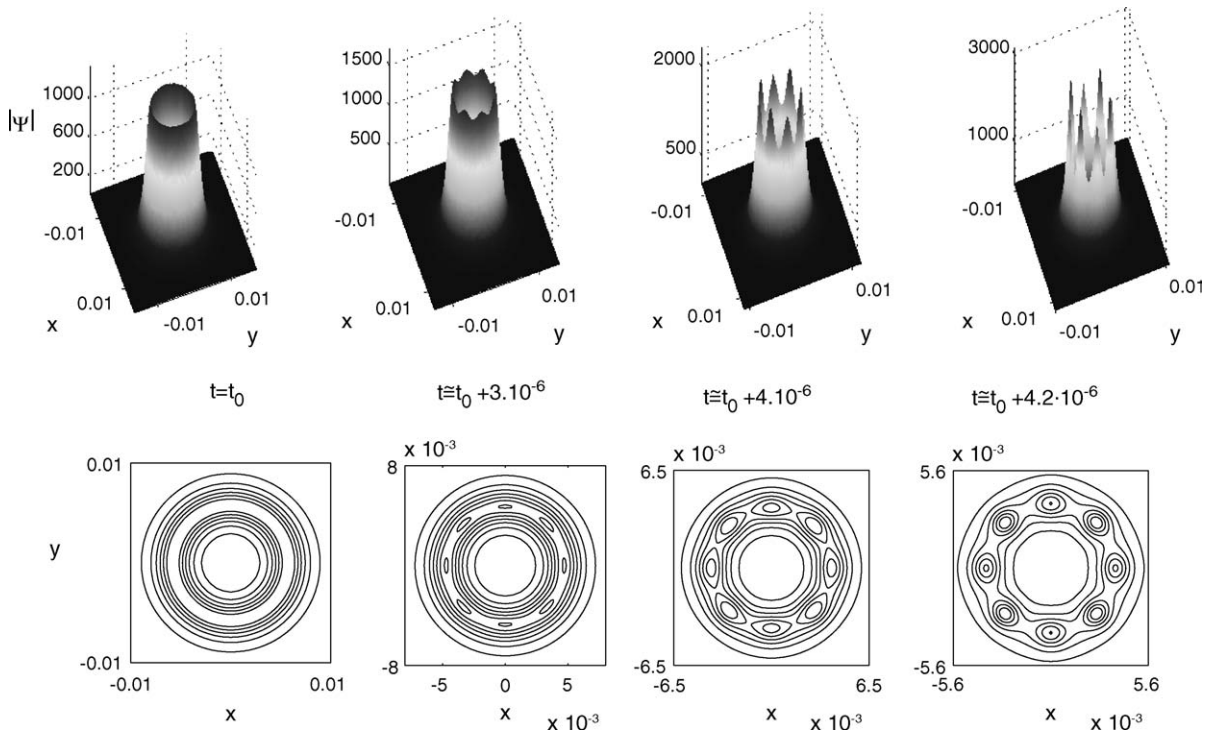

Fig. 23. Solution of the NLS (1) with the slightly elliptic single ring profile (31). Top: Surface plot. Bottom: Level sets of $|\psi|$.

(28) up to $t = t_0 = 7.8185$, such that $A(t_0) = 1000$. Then, we add small ellipticity ($\varepsilon = 0.01$) to the solution at t_0 and use it as an initial condition for the simulation of the NLS (1). In other words, we solve the NLS (1) with the initial condition

$$\psi(t_0, x, y) = \psi_G\left(t_0, r = \sqrt{x^2 + 1.01y^2}\right). \tag{31}$$

As Fig. 23 shows, the ring breaks into eight filaments located along a circle $r = r_{\text{fil}}$. These eight filaments consist of a pair of identical filaments located at $(\pm r_{\text{fil}}, 0)$, another pair of identical filaments located at $(0, \pm r_{\text{fil}})$ and a quadruple of identical filaments located at $(\pm x_{\text{fil}}, \pm y_{\text{fil}})$ such that $x_{\text{fil}}^2 + y_{\text{fil}}^2 = r_{\text{fil}}^2$.[9] Therefore, the collapsing ring profile is unstable as a solution of the NLS (1), i.e., with respect to perturbations that breakup the radial symmetry.

6.2.2. Elliptic super-Gaussian initial conditions

In the radially-symmetric case, we saw that high-power super-Gaussian initial conditions collapse with a single ring self-similar profile (Figs. 2–4). To check the stability of such solutions under symmetry-breaking perturbations, we solve the NLS (1) with the elliptic super-Gaussian initial condition,

$$\psi_0(x, y) = 10\, \mathrm{e}^{-(x^2+1.01y^2)^2},$$

[9] As was pointed out in [25], since the NLS (1) is isotropic, the symmetry breaking induced by ellipticity preserves the symmetries $x \to -x$ and $y \to -y$. Therefore, the filamentation pattern induced by ellipticity can only consist of single on-axis filament, pairs of identical filaments located along the ellipse major axis at $(\pm x, 0)$, pairs of identical filaments located along the minor axis at $(0, \pm y)$, and quadruples of filaments located at $(\pm x, \pm y)$.

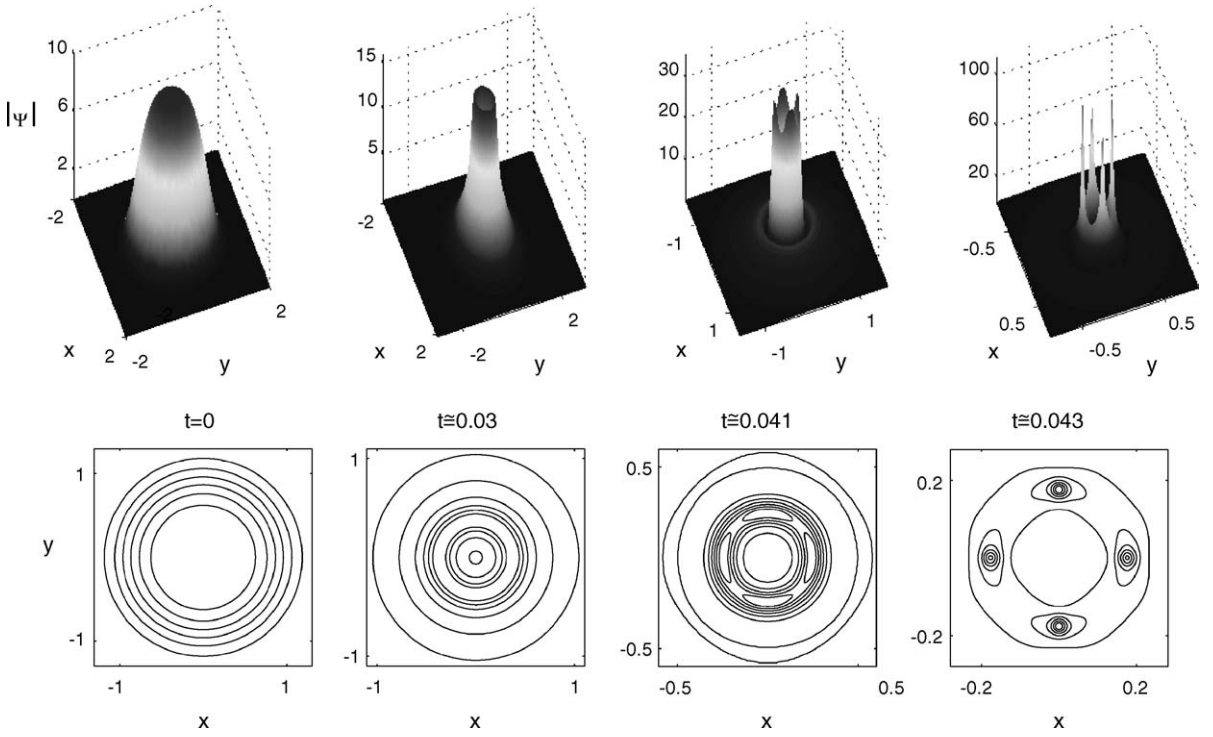

Fig. 24. Same as Fig. 23 for the initial condition $\psi_0 = 10\,\mathrm{e}^{-(x^2+1.01y^2)^2}$.

for which $N(0) = 16.82$. The slightly elliptic super-Gaussian initial condition initially evolves into a ring structure. However, after focusing by about 4, the ring breaks into four filaments located along a circle $r = r_{\mathrm{fil}}$, see Fig. 24. For comparison, in the radially-symmetric case $\varepsilon = 0$, this solution collapses with a ring-profile up to focusing levels of $A(t) = \mathcal{O}(10^{15})$ (see Fig. 19). As in Fig. 23, one pair of identical filaments is located at $(\pm r_{\mathrm{fil}}, 0)$ and another pair of identical filaments is located at $(0, \pm r_{\mathrm{fil}})$.

7. Supercritical NLS

The NLS Eq. (10) can be written in a more general form as

$$\mathrm{i}\psi_t(t,r) + \psi_{rr} + \frac{d-1}{r}\psi_r + |\psi|^2\psi = 0, \qquad \psi(0,r) = \psi_0(r). \tag{32}$$

The case $d > 2$ is known as the supercritical NLS. Since the supercritical NLS also admits singular solutions, it is natural to ask whether collapsing ring solutions also exist in the supercritical case. To do that, we solve the supercritical NLS (32) with a super-Gaussian initial condition of the form $\psi_0 = 10\,\mathrm{e}^{-r^4}$. As in the critical case, the solution collapses with a ring structure (see Fig. 25A). However, if we normalize the supercritical ring solution according to Eq. (13), the normalized ring expands as the solution collapses (See Fig. 25B). This shows that, unlike the critical case, the rate at which ring amplitude increases is faster than the rate at which the ring radius shrinks. We also observe that the expansion rate of the rescaled ring is $\approx L^{1/2}$. Therefore, the amount of power collapsing into the singularity $\inf_\varepsilon \lim_{t\to T_c} \int_{|x|<\varepsilon} |\psi|^2 r^2 \mathrm{d}r$ is zero (i.e., weak collapse). In contrast, for the ring blowup solutions of the critical NLS (1) the amount of power collapsing into the singularity is positive (strong collapse). We thus see

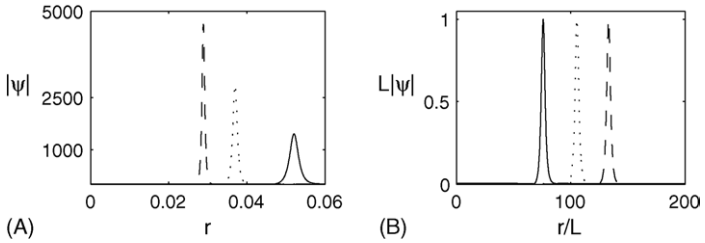

Fig. 25. (A) Solution of the supercritical NLS (32) for $d = 3$, with $\psi_0 = 10\,e^{-r^4}$ at $t = 0.38711$ (solid), $t = 0.03872$ (dots) and $t = 0.038723$ (dashes). (B) Same data as in A, normalized according to Eq. (13).

that collapsing ring profiles of the supercritical NLS (32) do exist, but that they are quite different from those of the critical NLS. A systematic study of these solutions will be presented elsewhere.

8. Do collapsing ring solutions exist in H^1?

In Section 4.3 we have found explicit self-similar ring solutions that blowup at a square root rate, which we denoted by $\psi_G^{(ex)}$, see (26). These solutions, however, have an infinite power (L^2 norm). This raises the question whether there exist H^1 solution of the NLS that collapse with a ring profile at a square root rate. Our simulations with high power super-Gaussian initial conditions (which are in H^1) show that they collapse with a self-similar ring profile at a square-root blowup rate, up to focusing levels of 10^{16}. At higher focusing levels our numerical code becomes unreliable. Even if we could reach somewhat higher focusing levels, it would not be possible to determine numerically whether ring solutions of the NLS, such as the ones that we presented in this study, will maintain a ring profile until the singularity. One could attempt to "overcome" this limitation by trying to extrapolate the results of Fig. 19 to power levels of $N = \mathcal{O}(50N_c)$. Unfortunately, it is not clear whether the focusing level at the transition to the Townes profile will be finite but exceedingly huge (e.g., 10 to the power of several hundreds of thousands), or whether the solution would maintain a ring profile all the way until the singularity. Therefore, the question whether there exist blowup solutions in H^1 with a self-similar ring profile has to be answered using analytic arguments.[10]

We have seen that the self-similar ring profile is given by the G-profile (Proposition 1), and that the power of G is infinite (Lemma 5). This seems to suggest that finite power (or H^1) collapsing ring solutions do not exist. However, as the simulations of Section 5 show, the self-similar profile ψ_G characterizes only the collapsing ring region and not the whole solution,[11] i.e.,

$$\psi(t,r) \sim \begin{cases} \psi_{\text{inner}} & 0 \le r < \rho_1 L(t) \\ \psi_G & \rho_1 L(t) \le r \le \rho_2 L(t) \\ \psi_{\text{outer}} & \rho_2 L(t) < r \end{cases}, \tag{33}$$

with $\rho_2 \gg \rho_1 \gg 1$ and $L(t) = 1/\max_{x,y} |\psi(t,x,y)|$. Thus, the assumption made in Proposition 1 that the solution is self-similar for $0 \le r \le \infty$ is valid only for non-H^1 solutions, such as $\psi_G^{(ex)}$.[12] In the case of H^1 solutions,

[10] Whether the self-similar ring profile is maintained "only" for focusing over several hundreds (or thousands) orders of magnitudes or all the way until the singularity is "only" a mathematical issue. Indeed, for any conceivable application, the validity of the NLS as a physical model breaks down long before reaching focusing levels of 10^{16}.

[11] This partial beam collapse property also characterizes NLS solutions that blowup with the R-profile, see (8).

[12] Indeed, a whole beam collapse for H^1 solutions is not possible when $H(|\psi_0|) \neq 0$ [26].

Proposition 1 applies only to the ring region, since only there the solution is characterized by a self-similar profile. The "modified" version of Proposition 1 for H^1 *quasi self-similar* solutions is as follows:

Proposition 13. *Let ψ be a singular solution of the NLS (1) with an asymptotic quasi self-similar blowup profile (33), where ψ_G is given by (14). Assume that (15) holds. Then, $G(\xi)$ is the solution of*

$$G''(\xi) + \frac{G'}{\xi} + \left[\frac{\alpha^4}{16}\xi^2 - 1\right] G + G^3 = 0, \quad \text{for } \rho_1 \le \xi \le \rho_2. \tag{34}$$

Proof. The proof is exactly the same as the proof of Proposition 1, simply applied only to the bounded region $\rho_1 L(t) \le r \le \rho_2 L(t)$. □

Of course, Proposition 13 does not prove the existence of H^1 ring solutions, since it relies on the assumption that the solution has the quasi self-similar blowup profile (33). While our numerical results support this assumption, the validity of the this assumption should be confirmed analytically, e.g., by calculating ψ_{inner} and ψ_{outer}, and matching them with ψ_G.

Proposition 13 shows that the behavior of ψ for $\xi \gg \rho_2$ is not characterized by the ring profile G. Indeed, since the ring solution amplitude decays at large ξ (see Lemma 5), at $\xi \gg \rho_2$ the NLS reduces to the linear Schrödinger equation $i\psi_t(t, x, y) + \Delta\psi = 0$. Therefore, the infinite-power "tail" of the ring profile G is "irrelevant" to the NLS ring solutions, as can be seen in Fig. 15D–F. We note that the feature of the "irrelevant infinite power tail" also occurs in the supercritical NLS (32). Indeed, H^1 blowup solutions of the super-critical NLS collapse with an asymptotic self-similar which is known as the Q profile [12,27]. As in the case of the G profile, the overall power of Q between $\xi = 0$ and $\xi = \infty$ is infinite. However, the simulations and analysis in [28,29] show that the collapse is, in fact, only quasi self-similar, with linear propagation for sufficiently large ξ. Hence, the quasi self-similar Q profile is consistent with an overall finite power of the collapsing solution. The same feature was also observed and analyzed by Malkin [30] in the critical case for solutions that blow up with the Townes profile.

In summary, at present, the numerical and analytical results do not provide a conclusive answer to whether collapsing ring solutions exist in H^1. For further discussion on this issue, see Section 9.

9. Final remarks

In this study, we presented NLS simulations of solutions that blowup with a quasi self-similar ring profile at a square-root blowup rate up to focusing levels of 10^{16}, at which point our numerical code may become unreliable. As we noted in Section 8, the question whether there exist collapsing H^1 solutions that maintain a ring solution and blowup at a square root blowup rate all the way up to singularity is still open. As we have seen, existence of such solutions does not contradict the recent results of Merle and Raphael (see Section 5.3) nor the infinite power of the G-profile (Section 8).

Several open issues, which are related to the question of existence of H^1 ring solutions, are:

- The assumption that the ring solution is quasi self-similar of the form (33) (see Section 8) is strongly supported by the numerical results, but its validity at focusing level $\gg 10^{16}$ is an open question.
- The minimal tail criteria for determining the relation $\alpha = \alpha^{(1)}(G_0)$ for single ring G-profiles (see Section 4) is reasonable as an initial choice, but the correct criteria could be based on matching between ψ_G and ψ_{outer}.
- What is the minimal power for a ring-type collapse (see Section 5.3)?

As we have noted, at present, the numerical and analytical results do not provide a conclusive answer to whether collapsing H^1 ring solutions of the critical NLS maintain a ring-profile all the way up to the singularity. It they do,

they represent a new type of singular solutions of the critical NLS. If, however, these ring solutions will change into R profiles at exceedingly high focusing levels ($\gg 10^{16}$), these ring solutions represent a new type of "quasi-singular" solutions of the critical NLS. We note that this distinction between truly singular ring solutions and "quasi-singular" ring solutions is a mathematical issue, since for any conceivable physical application, the NLS model is not valid at focusing levels which are $\gg 10^{16}$.

Finally, we note that ring-type collapse was recently observed in experiments with high-power, flattened-top laser beams [31]. These experiments were preliminary and considered only the early stages of the ring creation. Since our simulations show that as the rings collapse they become unstable with respect to symmetry-breaking perturbations (see Section 6), a more detailed experimental investigation is needed to study the issue of ring stability at higher focusing levels.

Acknowledgement

Partially supported by grant 2000311 from the United States–Israel Binational Science Foundation, Jerusalem, Israel.

Appendix A. Calculation of the G-profile (16)

Lemma 5 ensures that all solutions of Eq. (16) decay as $\xi \to \infty$. Therefore, we can solve Eq. (16) as an initial value problem with the conditions $G(0) = G_0$ and $G'(0) = 0$ using a standard Runge-Kutte ODE solver.

Appendix B. Calculation of c_G

In order to calculate c_G, we first find the locations $0 < \xi_1 < \xi_1 < \xi_3 < \cdots$ of the local maxima of $|\psi|$. From Lemma 5 we know that

$$|G(\xi_n)| \sim \frac{c_G}{\xi_n}, \qquad \xi_n > \frac{1}{\alpha^2}. \tag{B.1}$$

Therefore, we perform a linear data fit for the series of points $\{(\xi_n, 1/G(\xi_n))\}$ for $\xi_n > 1/\alpha^2$. The slope of the fitted line is c_G^{-1}.

Appendix C. Finding $a^{(n)}(G_0)$

Given $G_0 = G(0)$, we want to find $\alpha^{(1)}(G_0)$, i.e., the value of α for which the solution of (16) will be a ring solution with the smallest oscillation tail possible. A direct method would be to first find a value of α than corresponds to a solution with a single-ring (with a non-small tail) and then minimize c_G as a function of α, where c_G is calculated as in Appendix B. This approach demands a good initial guess for $\alpha^{(1)}(G_0)$ and turns out to be relatively inefficient.

A better approach is to look at the value of $G(\xi_2)$ where $\{\xi_n\}$ is the series defined in Appendix B. For a single-ring solution, ξ_2 already belongs to the oscillating tail, therefore we expect $|G(\xi_2)|$ to be minimal. Naively, a minimum finding algorithm can be applied to find the optimal α which minimizes $|G(\xi_2)|$. However, a better approach can be derived by noting that as α changes from $\alpha^{(1)} - \varepsilon$ to $\alpha^{(1)} + \varepsilon$, $G(\xi_2)$ changes its sign (see Fig. 10 and also Fig. C.1). We can take advantage of this property and apply a zero-finding algorithm to find the value for which $G(\xi_2)$ is closest to zero. This method is significantly faster than the minimum finding algorithm and in addition it does not demand a good initial guess for $\alpha^{(1)}(G_0)$. Clearly, since Lemma 5 ensures that c_G can not be zero, $G(\xi_2)$ cannot

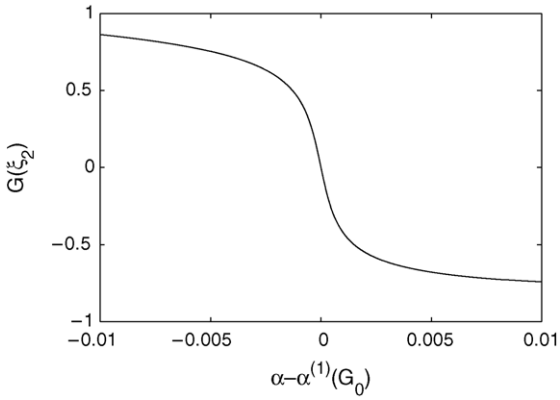

Fig. C.1. $G(\xi_2)$ as a function of $\alpha - \alpha^{(1)}(G_0)$ for $G_0 = 0.0003$.

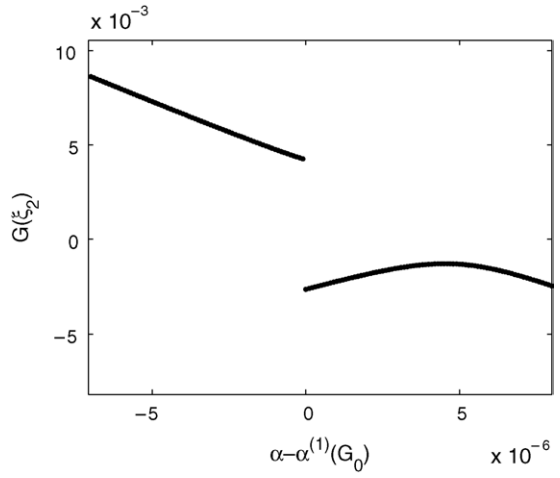

Fig. C.2. Zoom-in on Fig. C.1 near $\alpha = \alpha^{(1)}(G_0)$.

be zero as well. Indeed, zooming in on the neighborhood of $\alpha^{(1)}(G_0)$ shows a discontinuity at $\alpha = \alpha^{(1)}$ (Fig. C.2). The discontinuity in the graph asserts that the zero finding algorithm will be stopped by an external threshold and not when finding a true optimal value. This does not constitute a problem, however, because as Fig. C.2 shows, the zero search will terminate at a value of α which is $\mathcal{O}(10^{-6})$ close to $\alpha^{(1)}(G_0)$.

Extension of the method to n-ring solutions is done searching for the values of $\alpha = \alpha^{(n)}(G_0)$ for which $G(\xi_{n+1})$ is closest to zero.

Appendix D. Matching a given ring profile with a G-profile

When we find a self-similar ring profile of a collapsing NLS solution, we would like to find the corresponding best fitting single-ring solution of (16). To do that, we first require that the two profiles will have the same amplitude by normalizing ψ and the G-profile according to (13). Fig. D.1 shows that the radius of the normalized G-profiles

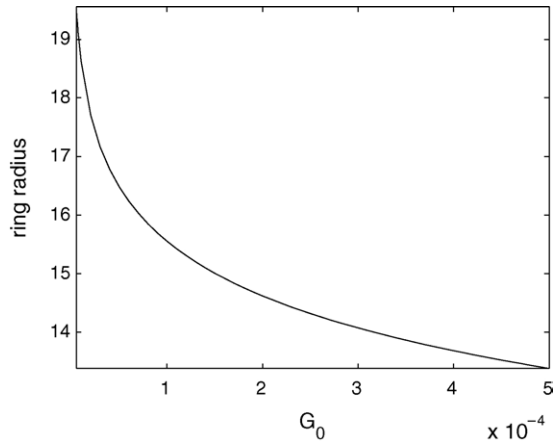

Fig. D.1. Radius of a normalized single-ring G-profile as a function of G_0.

increases monotonically as G_0 decreases (as, of course, can be expected). Therefore, the match is done by searching for the value of G_0 for which the normalized G and ψ and have the same radius.

Appendix E. Simulation of radially-symmetric NLS (dynamic rescaling)

Simulations of the radially-symmetric NLS (10) were performed using the method of dynamic rescaling [9] with approximate boundary conditions [32]. In this method, the independent variables and the function are dynamically rescaled in a way which is based on the asymptotic form of the solution (14). As a result, in the rescaled variables, the function is smooth and the problem can be solved on a fixed grid using standard techniques. Finally, the NLS solution is recovered from that of the rescaled problem. Additional rescaling is applied to the modulation variables L and τ, so that they match the corresponding variables of the asymptotic theory [1,33].

Appendix F. Simulation of anisotropic NLS (iterative grid redistribution)

We use the iterative grid redistribution method for the simulations of the NLS with anisotropic initial conditions. The IGR method was introduced in [34] and further improved in [35] and [36]. The method consists of the following three parts:

(1) A grid generation rule that determines the mesh mapping $\mathbf{x} = T(\xi)$.
(2) An iterative procedure that controls the grid distribution near the singular points.
(3) A procedure for solving the NLS.

Step (2) is the key for the method to be successful for the problem with singular behavior. It is a procedure that improves the grid distribution near singular region if the mapping T in step (1) cannot achieve enough resolution in the singular region. In step (1), the grid generation in two and three spatial dimensions is commonly done using the variational approach, specifically by minimizing a functional of the coordinate mapping between the physical domain and the computational domain. The functional is chosen so that the minimum is suitably influenced by the desired properties of the solution of the PDE itself. Steps (1) and (2) are then incorporated into a static adaptive method for solving the NLS equation in the computational domain. The grid re-generation is needed when certain

smoothness criterion for the solution in the computational domain is violated. The advantage of the method is that it can handle singularities with complicated structures. For details, we refer the reader to [35,34,36].

References

[1] G. Fibich, G. Papanicolaou, Self-focusing in the perturbed and unperturbed nonlinear Schrödinger equation in critical dimension, SIAM J. Appl. Math. 60 (1999) 183–240.
[2] W. Strauss, Nonlinear Wave Equations, American Mathematical Society, Providence, R.I, 1989.
[3] C. Sulem, P. Sulem, The Nonlinear Schrödinger Equation, Springer, New-York, 1999.
[4] M. Grillakis, Existence of nodal solutions of semilinear equations in $\mathbb{R}^N$, J. Differ. Equations 85 (1990) 367–400.
[5] R. Chiao, E. Garmire, C. Townes, Self-trapping of optical beams, Phys. Rev. Lett. 13 (1964) 479–482.
[6] M. Weinstein, Nonlinear Schrödinger equations and sharp interpolation estimates, Commun. Math. Phys. 87 (1983) 567–576.
[7] V. Talanov, Focusing of light in cubic media, JETP Lett. 11 (1970) 199–201.
[8] M. Landman, G. Papanicolaou, C. Sulem, P. Sulem, X. Wang, Stability of isotropic singularities for the nonlinear Schrödinger equation, Physica D 47 (1991) 393–415.
[9] D. McLaughlin, G. Papanicolaou, C. Sulem, P. Sulem, Focusing singularity of the cubic Schrödinger equation, Phys. Rev. A 34 (1986) 1200–1210.
[10] G. Fraiman, Asymptotic stability of manifold of self-similar solutions in self-focusing, Sov. Phys. JETP 61 (1985) 228–233.
[11] M. Landman, G. Papanicolaou, C. Sulem, P. Sulem, Rate of blowup for solutions of the nonlinear Schrödinger equation at critical dimension, Phys. Rev. A 38 (1988) 3837–3843.
[12] B. LeMesurier, G. Papanicolaou, C. Sulem, P. Sulem, The focusing singularity of the nonlinear Schrödinger equation, in: M. Grandall, P. Rabinovitz, R. Turner (Eds.), Directions in Partial Differential Equations, Academic Press, New-York, 1987, pp. 159–201.
[13] M. Weinstein, The nonlinear Schrödinger equation—singularity formation, stability and dispersion, Contemp. Math. 99 (1989) 213–232.
[14] H. Nawa, Asymptotic profiles of blow-up solutions of the nonlinear Schrödinger equation with critical power nonlinearity, J. Math. Soc. Jpn. 46 (1994) 557–586.
[15] H. Nawa, Asymptotic and limiting profiles of blow-up solutions of the nonlinear Schrödinger equation with critical power, Commun. Pure Appl. Math. 52 (1999) 193–270.
[16] F. Merle, P. Raphael, Sharp upper bound on the blow-up rate for the critical nonlinear Schrödinger equation, Geom. Funct. Anal. 13 (2003) 591–642.
[17] F. Merle, P. Raphael, On universality of blow-up profile for L^2 critical nonlinear Schrödinger equation, Invent. Math. 156 (2004) 565–672.
[18] F. Merle, P. Raphael, Profiles and quantization of the blow up mass for critical nonlinear Schrödinger equation, Commun. Math. Phys. 253 (2005) 675–704.
[19] K. Moll, A. Gaeta, G. Fibich, Self-similar optical wave collapse: Observation of the Townes profile, Phys. Rev. Lett. 90 (2003) 203902.
[20] L. Bergé, C. Gouédard, J. Schjodt-Eriksen, H. Ward, Filamentation patterns in Kerr media vs. beam shape robustness, nonlinear saturation and polarization states, Physica D 176 (2003) 181–211.
[21] C.J. Budd, Asymptotics of multibump blow-up self-similar solutions of the nonlinear Schrödinger equation, SIAM J. Appl. Math. 62 (2001) 801–830.
[22] T. Cazenave, F. Weissler, The Cauchy problem for the nonlinear Schrödinger equation in H^1, Manuscripta Math. 81 (1988) 477–498.
[23] F. Merle, Lower bounds for the blow-up rate of solutions of the Zakharov equation in dimension two, Commun. Pure Appl. Math. 49 (1996) 765–794.
[24] R. Johnson, X. Pan, On an elliptic equation related to the blow-up phenomenon in the nonlinear Schrödinger equation, Proc. R. Soc. Edinburgh Sect. A 123 (1993) 763–782.
[25] A. Dubietis, G. Tamošauskas, G. Fibich, B. Ilan, Multiple filamentation induced by input-beam ellipticity, Opt. Lett. 29 (2004) 1126–1128.
[26] H. Nawa, M. Tsutsumi, On blow-up for the pseudo-conformally invariant nonlinear Schrödinger equation, Funkcial. Ekvac. 32 (1989) 417–428.
[27] B. LeMesurier, G. Papanicolaou, C. Sulem, P. Sulem, Local structure of the self-focusing singularity of the nonlinear Schrödinger equation, Physica D 32 (1988) 210–226.
[28] L. Bergé, D. Pesme, Time dependent solutions of wave collapse, Phys. Lett. A 166 (1992) 116–122.
[29] V. Shvets, N.E. Kosmatov, B.J. LeMesurier, On collapsing solutions of the nonlinear Schrödinger equation in the supercritical case, in: R. Caflisch, G. Papanicolaou (Eds.), Singularities in Fluids, Plasmas and Optics, NATO ASI Series, vol. 404, Kluwer Academic Publishers, 1993, pp. 671–692.
[30] V. Malkin, Dynamics of wave collapse in the critical case, Phys. Lett. A 151 (1990) 285–288.
[31] T. Grow, A. Gaeta, G. Fibich, Observation of new singular solutions of the nonlinear Schrödinger equation, Nonlinear Guided Waves and Their Applications (NLGW 2005), FC4, 6–7 September 2005, Dresden, Germany.

[32] N. Kosmatov, V. Shvets, V. Zakharov, Computer simulation of wave collapses in the nonlinear Schrödinger equation, Physica D 52 (1991) 16–35.
[33] G. Fibich, Self-focusing in the nonlinear Schrödinger equation for ultrashort laser-tissue interactions, Ph.D. thesis, Courant Institute, NYU, 1994.
[34] W. Ren, X. Wang, An iterative grid redistribution method for singular problems in multiple dimensions, J. Comput. Phys. 159 (2000) 246–273.
[35] G. Fibich, W. Ren, X. Wang, Numerical simulations of self focusing of ultrafast laser pulses, Phys. Rev. E 67 (2003) 056603.
[36] D. Wang, X. Wang, A three-dimensional adaptive method based on the iterative grid redistribution, J. Comput. Phys. 199 (2004) 423–436.